Importance of PbI_2 morphology in two-step deposition of $CH_3NH_3PbI_3$ for high-performance perovskite solar cells*

Hui Wei(韦慧)[1,2], Yang Tang(汤洋)[1,†], Bo Feng(冯波)[1], and Hui You(尤晖)[2]

[1] Beijing Engineering Research Center of Nano-structured Thin Film Solar Cell, National Institute of Clean-and-Low-Carbon Energy, Beijing 102209, China
[2] Institute of Intelligent Machines, Chinese Academy of Sciences, Hefei 230031, China

(Received 26 June 2017; revised manuscript received 23 August 2017; published online 20 October 2017)

Controlling the morphology of the perovskite film is an effective way to improve the photoelectric conversion efficiency of solar cell devices. In this work, we study the influence of the crystallization condition on PbI_2 morphology and the performances of resulting perovskite solar cells. The PbI_2 morphologies and coverage rates under different formation conditions such as solvent effect, slow crystallization at room temperature and substrate-preheating, are found to be of crucial importance for preparing high-quality perovskite. The generation of loosely packed disk-like PbI_2 film with interpenetrating nanopores promotes the penetration of methyl ammonium iodide (MAI), leading to a better crystallinity of the perovskite film, and a best repeatable power conversion efficiency of 11.59% is achieved when methyl ammonium lead triiodide ($CH_3NH_3PbI_3$, $MAPbI_3$) is employed. In addition, an excellent device is also obtained with an efficiency of more than 93% to remain after working for 43 days.

Keywords: morphology, PbI_2 solution, perovskite, solar cells, crystallization

PACS: 88.40.hj, 84.60.Jt, 78.56.–a **DOI:** 10.1088/1674-1056/26/12/128801

1. Introduction

Hybrid organic–inorganic perovskite, the chemical general formula ABX_3 ($A = CH_3NH_3$, $HC(NH_2)_2$, Cs; B = Pb, Sn; X = Cl, Br, I) perovskite family, is a well-known material with excellent absorption coefficient,[1,2] long carrier diffusion length,[3–5] high mobility,[6,7] and a tunable bandgap.[8–10] These properties can be tuned by changing the A, B, and X atoms. Nowadays, the certified efficiency of a hybrid organic–inorganic perovskite solar cell (PSC) has already reached up to 22.1%,[11] which proves that the hybrid organic–inorganic perovskite is a viable candidate for crystalline silicon solar cells and copper indium gallium selenide (CIGS) commercial photovoltaic (PV) devices, owing to its low-cost and facile solution-based fabrication process.

The perovskite film is at the core of PSC, whose quality greatly determines the photovoltaic performance. Many photo-physical properties, such as light harvesting, charge carrier transport and diffusion length, can be dramatically affected by the crystallization of the perovskite.[12–14] The defects and the crystal grain boundaries of the perovskite crystallites act as the traps of carriers, which aggravate the charge recombination. The current density–voltage (J–V) hysteresis effect, which causes inaccuracy in evaluating cell efficiency, is also believed to be related to the crystallinity and interfaces of the perovskite.[15,16] Thus, the performance of perovskite solar cell strongly depends on the morphology and composition.[17–22] So far, many methods have been exploited to prepare perovskite films with excellent photon and electron properties through tuning nucleation growth and the resulting micro-morphology of perovskite films.[23] Compared with the one-step method, the two-step method offers the good controlling of morphology, and it is much more economical and convenient than the vapor deposition method. For the two-step method, an inorganic halide (e.g., lead (II) iodide, PbI_2) layer is first deposited, whereupon organic ions (e.g., methyl ammonium iodide, MAI) are intercalated between the layers of edge sharing PbI_6 octahedra and form the perovskite. Burschka *et al.* used this two-step method to fabricate a perovskite solar cell in 2013,[24] wherein the spin-coated and dried PbI_2 layer was dipped in an appropriate 2-propanol solution with MAI. The process for PbI_2 deposition in the sequential deposition was found to be crucial to the final $MAPbI_3$ morphology and photovoltaic performance.[25] As a perovskite inorganic framework, the morphology of the original PbI_2 may affect the reproducibility of the photovoltaic performance because high-quality perovskite thin film depends on the morphology of the PbI_2 layer, dipping time, concentration and temperature of the MAI solution. In addition, the MAI penetration is a serious issue due to the volume expansion when the MAI is inserted into the PbI_2 crystal lattice.[25,26] This will lead to incomplete transformation of PbI_2 to perovskite on account of the fact that the initially formed $MAPbI_3$ compact layer blocks the MAI from being diffused and inserted into the PbI_2 layer. Moreover, the residual PbI_2 has detrimental effects on the carrier sepa-

*Project supported by the National Natural Science Foundation of China (Grant No. 61404007) and the Beijing Talents Fund, China (Grant No. 2015000021223ZK38).

†Corresponding author. E-mail: tangy118@hotmail.com

© 2017 Chinese Physical Society and IOP Publishing Ltd

ration and transportation. In the present work, we fabricate the materials with different surface morphologies (mainly surface coverage and different roughness) by adjusting the drying process of the PbI_2 layer.[26] Then the influences of synthesis conditions on the microstructures of perovskite films and the optical-electrical performances of the cells are investigated.

2. Solar cell fabrication

Patterned fluorine-doped tin oxide (FTO) substrates were cleaned in the solvents of detergent solution, acetone, ethanol and deionized water sequentially. Then the cleaned substrates were treated by UV-O_3 for 15 min to make them well hydrophilic. After that, 50-nm thick compact TiO_2 (c-TiO_2) was formed on the cleaned FTO glass by spin-coating 0.15-M solution of titanium diisopropoxide bis (acetylacetonate) (75 wt% in isopropanol, Aldrich) in 1-butanol (99.8%, Aldrich) at 3000 r.p.m for 30 s, which was dried at 125 °C for 5 min, then the process was repeated once again. A mesoporous TiO_2 (m-TiO_2) layer composed of 20 nm-sized particles was deposited by spin-coating at 3000 r.p.m for 30 s by using a commercial TiO_2 paste (18-NRT, Dyesol) diluted in ethanol (2:7, weight ratio). After drying at 125 °C for 10 min, the substrate was annealed at 500 °C for 30 min.

2.1. PbI_2 layer fabrication

PbI_2 (99.99%, Sigma-Aldrich) was dissolved in several kinds of polar solvents (N, N-dimethylformamide, DMF, > 99.9%, Sigma-Aldrich; N, N-dimethylsulfoxide, DMSO, 99.5%, Sigma-Aldrich) under stirring at 70 °C until its complete dissolution. The PbI_2 precursor solution was spin-coated on the substrates (FTO/c- TiO_2/m-TiO_2) at 3000 r.p.m for 30 s within an N_2 filled glovebox (deposition spinning details can be seen in Fig. 1). Also, different solutions used were simplified with A, B, C, and D, respectively, and then PbI_2 films with different solutions would be prepared after the coating process. The precursor solution of 1-M PbI_2 in DMSO and DMF/DMSO (92/8 v/v) mixture, which are marked with PbI_2-DMSO and PbI_2-DMF & DMSO, respectively. The preparation details of the PbI_2 precursor film with 1-M final concentration are shown in Table 1.

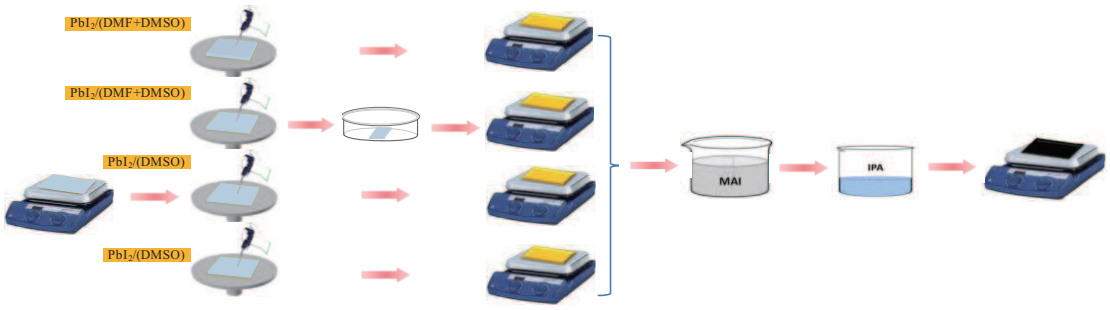


Fig. 1. (color online) A schematic diagram representation of the fabrication process.

Table 1. The PbI_2 precursor films prepared with different processes.

	Method	Precursor solution	PbI_2/g	PbI_2 film formation process
I	A	DMF & DMSO (92:8, v/v)	0.462	PbI_2 solution was deposited by spin coating at 3000 r.p.m for 30 s under an N_2 atmosphere within a glovebox, followed by immediately heating on a hot plate at 80 °C for 15 min.
	B	DMF & DMSO (92:8, v/v)	0.462	After the solution of PbI_2 was spin-coated, the wet film was kept in a covered Petri dish at room-temperature within a glovebox for 10 min and then heated on a hot plate at 80 °C for 5 min.
II	C	DMSO	0.462	Before a spin coating procedure the substrates were preheated at 80 °C, and the PbI_2 solution was deposited by repeating step a.
	D	DMSO	0.462	Repeating step a.

2.2. $MAPbI_3$ layer fabrication

To convert the PbI_2 layer into $MAPbI_3$, after cooling the substrates to room temperature, PbI_2 films were dipped into a solution of CH_3NH_3I (MAI, > 99.0%, Xi'an Polymer Light Technology Corp.) in 2-propanol (10 mg/ml) for 10 min, rinsed with 2-propanol and dried at 100 °C for 10 min. The 60-μl hole transport material (HTM) solution which consists of 72.3-mg Spiro-MeOTAD (2, 2′, 7, 7′-tetrakis-(N,N-di-4-methoxyphenylamino)-9, 9′-spirobifluorene, > 99%, Merck), 28.8 μl of 4-tert-butyl pyridine and 17.5 μl of lithium bis

(trifl uoromethanesulfonyl) imide (Li-TFSI, > 99.0%, Sigma-Aldrich) solution (520-mg Li-TSFI in 1-ml acetonitrile (99.8 %, Sigma-Aldrich)) in 1 ml of chlorobenzen, was spin-coated on the perovskite layer at 3000 r.p.m for 30 s. Finally, an Ag electrode was deposited by thermal evaporator at a constant evaporation rate of 5 Å/s.

2.3. Characterization

The x-ray diffraction measurements were performed on the D8 DISCOVER diffractometer (Bruker D8D, Germany) in grazing incidence x-ray diffraction (GIXRD) mode. The XRD patterns in a range from 10° to 60° were recorded at room temperature by using Cu Kα radiation under the following measurement conditions: a tube voltage of 40 kV, tube current of 40 mA, step size of 0.04°, and 20 s per step. The value of the grazing incidence angle was 0.05°. The absorption spectra of perovskite films were characterized by a UV-Vis-NIR spectrophotometer (SHIMADZU, UV3600) with an integrating sphere in the interval of 600 nm–900 nm. The photoluminescence (PL) spectra were measured by using an integrated Raman system (Horiba Jobin Yvon LabRam HR-800) with an Olympus 10X lens ($N_a = 0.25$). A 532-nm Nd-Yag laser (Laser Quantum, Torus 50 mW) was used as an excitation source and the wavelength scale was from 600 nm to 900 nm. The morphologies of perovskite films were observed by scanning electron microscopy (SEM, FEI Nova Nano 450). The current–voltage (J–V) characteristics of solar cells were measured with a fixed active area of 0.09 cm^2 by using a xenon (USHIO, UXL-150SO) based solar simulator lamp (Newport Oriel Sol 1A) and a Keithley 2420 source meter under 1-Sun illumination (AM 1.5G 1000 W/m^2) in air. All samples for characterization were prepared on the substrates FTO/c-TiO_2/m-TiO_2 with the same preparation procedure of thin films used in solar cells, unless otherwise stated.

3. Results and discussion

The PbI_2 morphology-related reaction kinetics in the two-step method is assigned to heterogeneous nucleation, which leads to the formation of PbI_2 nuclei on the m-TiO_2 stack layers. The liquid nature of the film, augmented by the presence of a large amount of solvent, leads to subsequent crystal growth, where the extent of growth is controlled by adjusting the nucleation density and growth condition. Figure 2 shows the top views of PbI_2 precursor films processed under different deposition conditions, each of which is composed of platelet-shaped PbI_2 crystals that are between 100 nm and 400 nm in diameter. It is clear that there is a big difference in surface morphology, which is due to their different fabrication processes. As seen clearly from Figs. 2(a) and 2(b), the slow crystallization process prefers to generate polyporous crystals because of the slow solvent evaporation. The drying process of PbI_2 film also helps to create larger pores and voids in the PbI_2 crystals which penetrate through the whole film. This porous morphology is probably related to the controlled slow solvent evaporation in the sealed box. These loose cavities can enhance the penetration of MAI in the PbI_2 layer during dipping, leading to the formation of perovskite. Thus, it can be seen that the morphology of the PbI_2 film is likely to be influenced by the low-temperature drying process. Compared with the nanoparticles in mixed solvent, the nanoparticles in pure DMSO solvent have sizes of 250 nm–400 nm and stack with a PbI_2 layer on the m-TiO_2 film as shown in Figs. 2(c) and 2(d). The majority of voids are formed within the PbI_2 layer, which is probably attributed to the high viscosity DMSO solvent and low nucleation density during the spin-coating process. Especially, the particulate network of PbI_2 is very much sparser in appearance (Fig. 2(d)), and the surface coverage on the TiO_2 film is smaller than that in the case of PbI_2 formed by using the substrate-preheating technique. The coverage seems to be related to competition between the solvent evaporation rate and the PbI_2 nucleation rate, that is, the PbI_2 nucleation rate becomes higher than the solvent evaporation rate because the substrate pre-heating process increases the nucleation sites. In the case of PbI_2 fabricated through process D, too much of a large gap forms in the grain and it is speculated that the $MAPbI_3$ films could not cover the substrates completely during the following deposition process, which will be discussed later in this work.

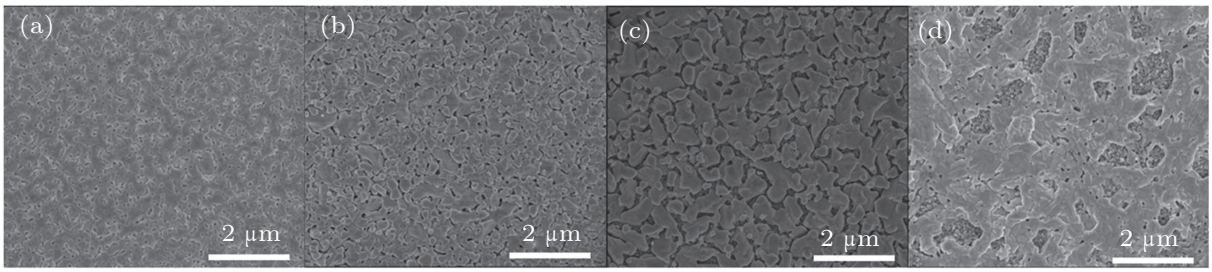


Fig. 2. SEM images of PbI_2 fabricated with method A, B, C, and D, respectively.

The DMSO acts as both a solvent and a coordination reagent in the formation of a complex of PbI_2·DMSO, while DMF behaves only as a solvent with a higher evaporation rate than DMSO (vapor pressure data are listed in Table 2). Because of the relatively low evaporation rate and high viscosity of pure DMSO, the coverage of the substrates is very poor,

which is unfavorable for the formation of perovskite in the second dipping step. Meanwhile, the coverage of PbI_2 film decreases if no pre-heating process is employed, which might be attributed to the hydrophobicity and large viscosity of DMSO. For mixed solvents, DMF solvent possesses a lower vapor pressure at room temperature which affects the morphology of the obtained PbI_2 film via the slow crystallization process.

Table 2. Typical physical parameters for DMF and DMSO solvents used for PbI_2 precursor.

Solvent	Density /(g/mL)	Boiling Point/°C	Viscosity /mPa·s	Vapor pressure /(mmHg, 20 °C)
DMF	0.948	152–154	0.92	2.7
DMSO	1.100	189	2.0	0.42

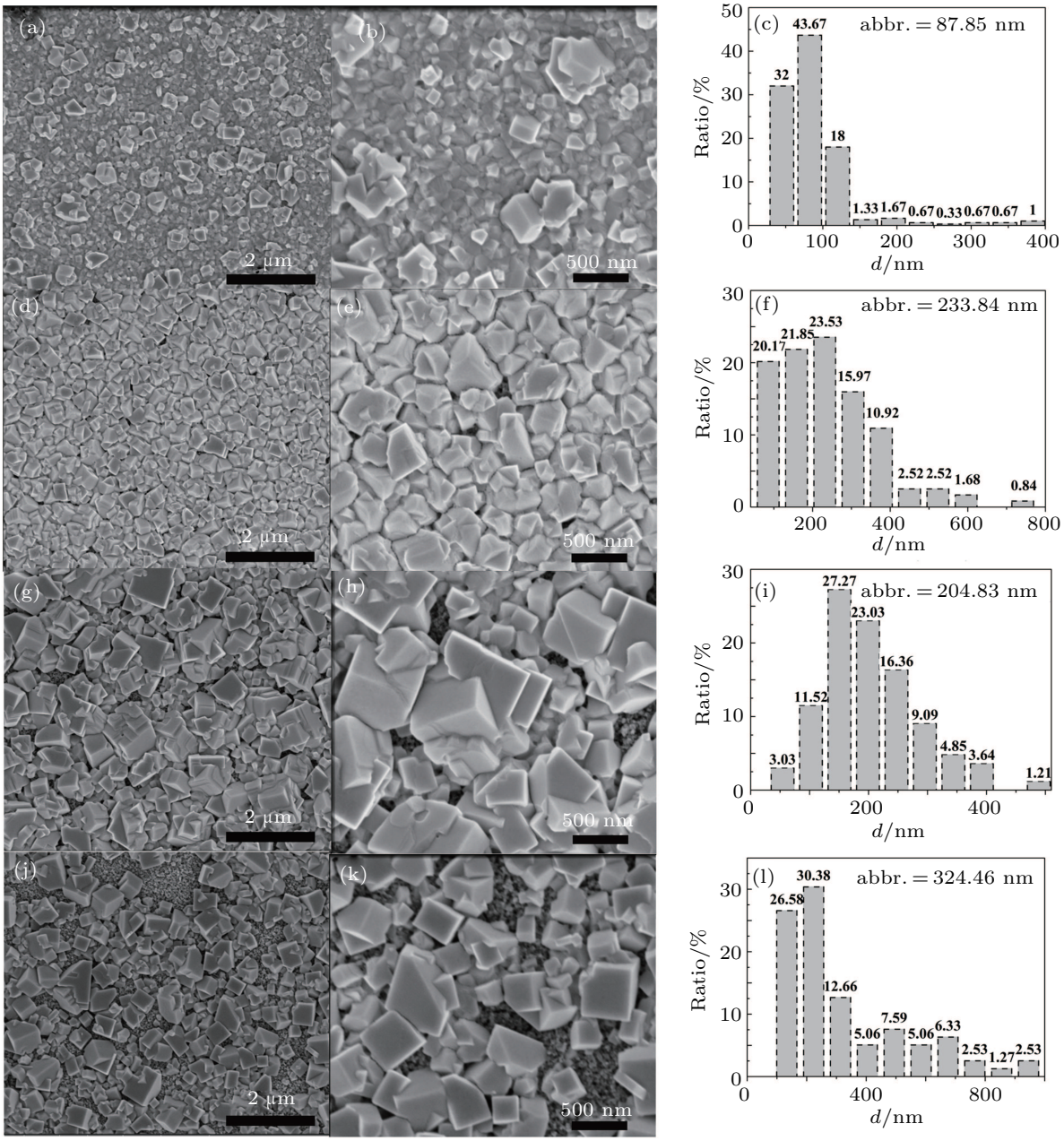


Fig. 3. SEM images of $MAPbI_3$ fabricated with different methods. ((a) and (b)) $MAPbI_3$ fabricated with method A; (c) the size analysis of the sample shown in panel (b); ((d) and (e)) $MAPbI_3$ fabricated with method B; (f) size analysis of the sample shown in panel (e); ((g) and (h)) $MAPbI_3$ fabricated with method C; (i) size analysis of the sample shown in panel (h); ((j) and (k)) $MAPbI_3$ fabricated with method D; (l) size analysis of the sample shown in panel k.

A series of $MAPbI_3$ films is prepared from different PbI_2 precursor films. For comparison, these perovskite thin films are denoted as PSC-a, PSC-b, PSC-c, PSC-d, respectively. Figure 3 shows the SEM images of the $MAPbI_3$ films prepared. It can be seen that the grain sizes and coverage rates of the resulting perovskite films change significantly. All the samples exhibit similar cuboid crystals. However, PSC-a and PSC-b overlayer have better quality than PSC-c and PSC-d in the aspect of smoothness and compactness, especially PSC-b is nearly pinhole-free and has a relatively uniform surface

(size distribution is shown in Fig. 3(f)). The PSC-a appears to be composed of small sized perovskite crystals ($\sim$ 80 nm), and its surface is covered with few uneven large cubic grain. The formation of coarse perovskite crystal usually appears during the Ostwald ripening process because of the dissolution-re-crystallization process (i.e., smaller perovskite crystals dissolve and re-deposit onto larger perovskite crystals). Obviously, the existence of slow crystallization at room temperature, with the same dipping time, is favorable for the large nanoparticles (cubic shape) on the surface $MAPbI_3$ film, an observation that is assistant and supports that the dense PbI_2 morphology impedes the penetration of MAI, so a portion of the formed small perovskites nanoparticles most likely continue to evolve by the above proposed mechanism.

In brief, the drying process at room temperature enhances the formation of larger pores in the PbI_2 film and larger $MAPbI_3$ particles, indicating the complete transformation of PbI_2 into $MAPbI_3$. In the case of pure DMSO used (PSC-c and PSC-d), the $MAPbI_3$ films are mainly composed of large crystals ($\sim$ 400 nm) filled with $\sim$ 100-nm small crystals, indicating the uneven coverage of the perovskite film. Without the preheating deposition, the gaps in perovskite film are formed (Fig. 3(k)) because localized nucleation gives rise to leakage current and direct contact between electron-and hole-transporting layers, resulting in serious charge recombination and deterioration of light absorption. These results reveal that the preheating of substrate has an important effect on PbI_2 spin coating through ameliorating the surface morphology and improving the quality of the resulting $MAPbI_3$ films.

Taking it into consideration that the reaction between PbI_2 and MAI is a solid–liquid reaction, we believe that the reaction rate is determined by three major factors: (i) property of PbI_2 film, such as preferential orientations of crystal, crystallinity and morphology of PbI_2 precursor film; (ii) concentration of MAI/IPA solution; (iii) temperature of the reaction system. In our study, the latter two factors have been carefully controlled. So we believe that the great difference among PbI_2 films in the preparation of perovskite comes from the morphology difference as shown in Fig. 2. Thus, controlling the morphology of PbI_2 may adjust the number of nuclei of the perovskite, and then affect the morphology of perovskite and grain size. We control the morphology of PbI_2 by adjusting the solvent polarity and drying process. Mainly, two main factors contribute to the faster conversion of nanoporous PbI_2 into perovskite rather than compact PbI_2: firstly, the interpenetrating nanoporous morphology enables the occurrence of reaction in the entire film simultaneously; secondly, the crystallite size is lower in the nanoporous PbI_2 than those in the compact PbI_2, shortening the diffusion length for MAI. In a word, the reaction is limited by the interface of PbI_2(s)–MAI (l) and fresh $MAPbI_3$, so the morphology of PbI_2 film is affected indeed in the two-step method because a large volume expansion occurs when PbI_2 converts into $MAPbI_3$ (about 74.8 cm^3–149.0 cm^3) due to the density difference between originally edge-sharing octahedral PbI_2 (6.16 g/cm^3) and the corner-sharing octahedral perovskite (4.29 g/cm^3).

In general, GIXRD is an effective tool to determine the surface crystallinity by changing the incident angle of x-ray. The samples are kept in a carefully controlled measurement condition, so the diffraction peak intensity is mainly determined by the crystallization, densification and components of the sample. The GIXRD patterns of the $MAPbI_3$ films obtained from PbI_2 are shown in Fig. 4. All film samples consisting of a cubic crystal phase possess similar patterns but with different diffraction intensities. The strong diffraction peaks at 14.21°, 20.68°, 24.57°, 28.52°, 31.90°, 35.04°, 40.62°, and 43.19° could be ascribed to (002), (022), (222), (004), (042), (422), (044), and (006) planes of the $MAPbI_3$ perovskite, respectively. Apart from the cubic character of an obvious perovskite phase with the space group of $F23$, a small number of PbI_2 phases exist in the PSC-d sample (the rose red curve in Fig. 4), and the peak at 12.73° corresponds to the (001) lattice plane of PbI_2, which indicates incomplete conversion of PbI_2. In combination with the SEM result, we speculate that the rough and nonuniform stacking nature of PbI_2 crystal retards the diffusion of MAI and therefore results in the subsequent incomplete conversion of PbI_2.

The higher intensity in the PSC-b film should be attributed to the slight thickness of the sample, or uniformly distributed nanocrystals and complete crystallization of the sample. Furthermore, the slight differences in lattice constant and full widths at half maximum (FWHMs) for different films imply that the PbI_2 precursor film only influences the perovskite film coverage and morphology without causing significant changes in the crystalline structure of the material.

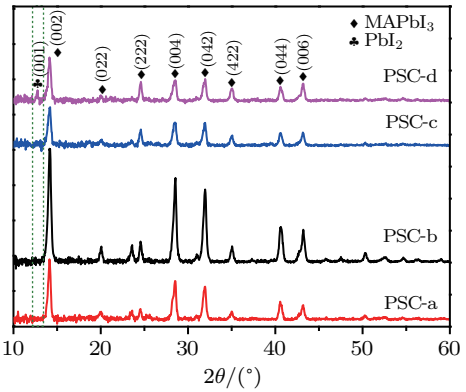


Fig. 4. (color online) XRD patterns of $MAPbI_3$ fabricated with methods A, B, C, and D, respectively.

Table 3 shows the lattice constants and FWHMs of the diffraction peak at $2\theta = 14.2°$. The average grain size D of

the $MAPbI_3$ nanocrystals can be estimated from the (002) peak at 14.2° by using the Scherrer equation: $D = k\lambda/(\beta\cos(\theta))$, where k is the Scherrer constant (equal to 0.89), λ is the x-ray wavelength (equal to 0.154 nm), θ is the Bragg diffraction angle, and β is the FWHM of the (002) diffraction peak. The FWHMs of the (002) diffraction peaks are 0.350, 0.381, 0.423, and 0.377, which correspond to average grain sizes of 22.6, 20.8, 18.7, and 21.0 nm for the PSC-a, PSC-b, PSC-c, and PSC-d sample, respectively.

Table 3. Lattice constants of $MAPbI_3$ films.

Sample	a/Å	Vol/Å^3	FWHM	Grain size
PSC-a	12.560	1981.385	0.350	22.6
PSC-b	12.578	1989.916	0.381	20.8
PSC-c	12.618	2008.961	0.423	18.7
PSC-d	12.582	1991.815	0.377	21.0

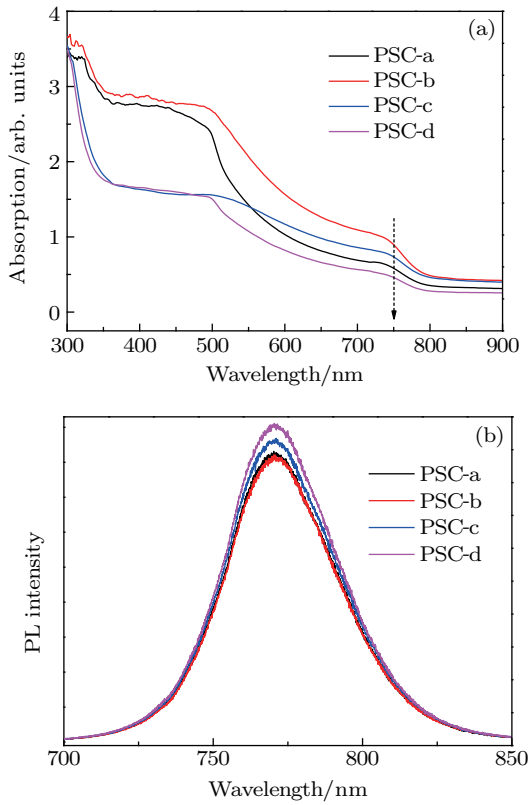


Fig. 5. (color online) (a) Absorption spectra and (b) PL spectra of $MAPbI_3$ films.

Figure 5 shows the absorption spectra and PL spectra of the corresponding PSC films. Their absorptions cover a wide range of light wavelengths from visible to the near-infrared region. All of these films exhibit the same absorption shoulders near 750 nm, which is typical nature for the $MAPbI_3$ phase. As a result of the poor coverage of the substrate by film when $MAPbI_3$ is prepared with pure DMSO solvent, their absorptions are lower than those of the $MAPbI_3$ fabricated with mixed solvents, which is more prominent in the short wavelength region (350 nm–550 nm). The PSC-b shows the most enhanced absorption, which is related to the improved morphology and coverage rate. In addition, it can be seen that $MAPbI_3$ films prepared with DMF/DMSO mixed polar solvent have strong absorptions, indicating that more PbI_2 nanoparticles are converted into $MAPbI_3$ nanoparticles. The increase in absorption supports that the loose structure assembled from PbI_2 nanoparticles allows MAI to reach the interior of PbI_2 very easily and facilitates the complete transformation of PbI_2. The characteristic absorption shoulder near 750 nm for PSC-c film increases slightly, which reflects the stronger light-scattering effect associated with abnormally large grains. This result reveals that good surface morphology of the $MAPbI_3$ film is important for the light absorption of the perovskite solar cell. Figure 5(b) shows the steady-state PL spectra of perovskite films excited at 532 nm. The PL quenches at around 776 nm, which is consistent with the behavior of the optical gap from the absorption spectra. These results suggest that the controlled growth of PbI_2 scaffolds could be a useful new route to manipulating the morphology of the perovskite active layer, opening new possibilities for enhancing device performance.

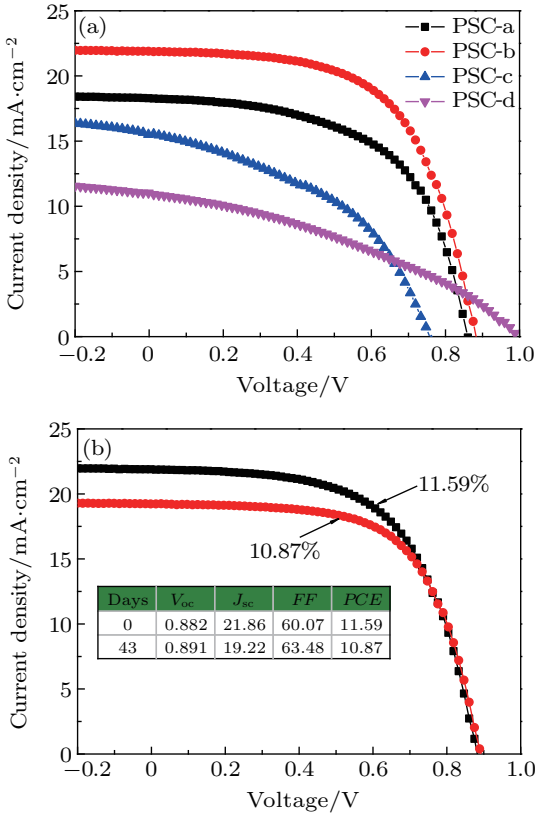


Fig. 6. (color online) (a) J–V curves of devices fabricated with different methods. (b) J–V curves of the best performance device fabricated by method B.

The photovoltaic performances of the fabricated PSCs based on FTO/c-TiO_2/m-TiO_2/$MAPbI_3$/HTM/Ag architecture are examined and the current–voltage (J–V) characteristics are

measured in the reverse bias condition (1.2 V→ −0.2 V) under standard AM 1.5G illumination, with an effective area of 0.09 cm^2. All the performance parameters such as short-circuit current density (J_{sc}), open circuit voltage (V_{oc}), fill factor (FF) and power conversion efficiency (PCE) are summarized in Table 4, which are achieved by a reverse bias scan. The solar cell with the PSC-b perovskite film exhibits a highest PCE performance of 11.59% with J_{sc} of 21.86 mA/cm^2, V_{oc} of 0.882 V and FF of 60.73 as expected. Meanwhile, the PCE of PCS-b keeps a high level of more than 93% of the initial efficiency (from 11.59% to 10.87%) after 43-day storage in air (Fig. 6(b)).

Table 4. Photovoltaic parameters of devices with different fabrication methods.

Fabrication methods	V_{oc}/V	J_{sc}/mA·cm^{-2}	FF	PCE_{best}/%
A	0.860	18.24	57.56	9.03
B	0.882	21.86	60.07	11.59
C	0.757	15.51	44.44	5.22
D	0.993	10.92	36.28	3.92

For mixed solvents, the higher PCE of PSC of the material prepared by method B is attributed to the PbI_2 scaffold with mesoporous structure, which promotes the conversion process of and less damage to perovskite. In addition, many studies have shown that a larger perovskite grain size can reduce the interfacial area, which can hinder charges from being collected. Larger grains also possess less bulk defects and higher mobilities, so the photo-generated carriers could be collected more easily.[27,28] We note that Yi *et al.*[29] reported solar cells based on bilayer porous lead halide (PbX_2, containing PbI_2 and $PbBr_2$) films prepared by using PbX_2 solutions of DMF/DMSO mixed-solvent. The MAI solution can easily diffuse through the PbI_2 film and react with PbI_2 more completely because of the continuous mesoporous structure. At the same time, these pores also provide the space needed to accommodate the large volume expansion and the insertion of the organic cations into the PbI_2 lattice. The interpenetrating nanoporous morphology enables fast penetration of the MAI solution during the conversion step, and perovskite grains can grow freely and form a compact $MAPbI_3$ film. For pure DMSO solvent, PCE of 3.92% is achieved without pre-heating and increases to 5.22% when the substrate is heated to 80 °C. The pre-heating treatment can lead to the increase of photocurrent and voltage. By contrast, the PbI_2-DMSO based device suffers relatively low J_{sc} and FF, which is attributed to the poor coverage with high leak current and low light-harvesting. The coverage of PbI_2 film on the m-TiO_2 layer decreases when only DMSO is used as solvent, because the hydrophobicity and high viscosity of DMSO make it difficult to spread on the substrate surface. In addition, since the substrate surface can provide nucleation sites for the nucleation of crystals, pre-heated substrate is likely to play a positive role in nucleating. And a higher coverage of perovskite layer is beneficial for the light absorption, leading to higher photocurrent and voltage.

4. Conclusions

In this work, a suitable polarity solvent, processed with and without drying at room temperature, pre-heating process of substrate for PbI_2 deposition in the two-step coating procedure, and the affinity to PbI_2, can facilitate the formation of mesoporous PbI_2 films and the fabrication of a uniform and crystalline perovskite film. In the case of full coverage and less pinholes of the perovskite film, excellent device efficiency and stability are achieved successfully. Meanwhile, the PCE of PCS-b keeps a high level of more than 93% (from 11.59% to 10.87%) after the cell has been used for 43 days under ambient conditions.

Acknowledgment

The authors thank the postdoctoral research station of the Hefei Institute of Physical Science for their technical support.

References

[1] Im J H, Jang I H, Pellet N, Gr?tzel M and Park N G 2014 *Nature Nanotechnology* **9** 927
[2] Sun S, Salim T, Mathews N, Duchamp M, Boothroyd C, Xing G, Sum T C and Lam Y M 2014 *Energy Environ. Sci.* **7** 399
[3] Stranks S D, Eperon G E, Grancini G, Menelaou C, Alcocer M J P, Leijtens T, Herz L M, Petrozza A, and Snaith H J 2013 *Science* **342** 341
[4] Dong Q F, Fang Y J, Shao Y C, Mulligan P, Qiu J, Cao L and Huan J S 2015 *Science* **347** 967
[5] Xing G H, Mathews N, Sun S Y, Lim S S, Lam Y M, Gr?tzel M, Mhaisalkar S, and Sum T C 2013 *Science* **342** 344
[6] Shi D, Adinolfi V, Comin R, Yuan M, Alarousu E, Buin A, Chen Y, Hoogland S, Rothenberger A, Katsiev K, Losovyj Y, Zhang X, Dowben P A, Mohammed O F, Sargent E H and Bakr O M 2015 *Science* **347** 519
[7] Lim K G, Ahn S Y, Kim Y H, Qi Y B and Lee T W 2016 *Energy Environ. Sci.* **9** 932
[8] Noh J H, Im S H, Heo J H, Mandal T N and Seok S I 2013 *Nano Lett.* **13** 1764
[9] Ogomi Y H, Morita A, Tsukamoto S T, Saitho T, Fujikawa N, Shen Q, Toyoda T, Yoshino K J, Pandey S S, Ma T L and S Hayase 2014 *J. Phys. Chem. Lett.* **5** 1004
[10] Jeon N J, Noh J H, Yang W S, Kim Y C, Ryu S C, Seo J W and Seok S Il 2015 *Nature* **517** 476
[11] NREL, Best Research-Cell Efficiencies, http://www.nrel.gov, accessed: November 2016
[12] Eperon G E, Burlakov V M, Docampo P, Goriely A and Henry J 2014 *Adv. Funct. Mater.* **24** 151
[13] Dualeh A, Tétreault N, Moehl T, Gao P, Nazeeruddin M K and Grätzel M 2014 *Adv. Funct. Mater.* **24** 3250
[14] Xiao Z G, Dong Q F, Bi C, Shao Y H, YuanY B, Huang J S 2014 *Adv. Mater.* **26** 6503
[15] Chen B, Yang M J, Priya S and Zhu K 2016 *J. Phys. Chem. Lett.* **7** 905
[16] Yuan Y B and Huang J S 2016 *Acc. Chem. Res.* **49** 286

[17] Li W Z, Fan J D, Li J W, Mai Y H and Wang L D 2015 *J. Am. Chem. Soc.* **137** 10399

[18] Zuo L J, Dong S Q, Marco N, Hsieh Y T, Bae S H, Sun P Y and Yang Y 2016 *J. Am. Chem. Soc.* **138** 15710

[19] Bi D Q, Yi C Y, Luo J S, Décoppet J D, Zhang F, Zakeeruddin S M, Li X, Hagfeldt A and Grätzel M 2016 *Nat. Energy* **1** 16142

[20] Saliba M, Matsui T, Domanski K, Seo J Y, Ummadisingu A, Zakeeruddin S M, Correa-Baena J P, Tress W R, Abate A, Hagfeldt A and Grätzel M 2016 *Science* **354** 206

[21] Park Y H, Jeong I, Bae S, Son H J, Lee P, Lee J, Lee C H and Ko M 2017 *J Adv. Funct. Mater.* **27** 1605988

[22] Huang F Z, Pascoe A R, Wu W Q, Ku Z L, Peng Y, Zhong J, Caruso R A and Cheng Y B 2017 *Adv. Mater.* **9** 1601715

[23] Zhou Y Y, Game O S, Pang S P and Padture N P 2015 *J. Phys. Chem. Lett.* **6** 4827

[24] Burschka J L, Pellet N, Moon S J, Humphry-Baker R, Gao P, Nazeeruddin M K and Grätzel M 2013 *Nature* **499** 316

[25] Yantara N, Sabba D, Yanan F, Kadro J M, Moehl T, Boix P P, Mhaisalkar S, Grätzeld M and Grätzel C 2015 *Chem. Commun.* **51** 4603

[26] Zhang T Y, Yang M J, Zhao Y X and Kai Zhu 2015 *Nano Lett.* **15** 3959

[27] Im J H, Jang J H, Pellet N, Grätzel M and Park N G 2014 *Nat. Nanotechnol.* **9** 927

[28] Nie W, Tsai H, Asadpour R, Blancon J C, Neukirch A J, Gupta G, Crochet J J, Chhowalla M, Tretiak S, Alam M A, Wang H L and Mohite A D 2015 *Science* **347** 522

[29] Yi C, Li X, Luo J, Zakeeruddin S M and Grätzel M 2016 *Adv. Mater.* **28** 2964